ACS OMEGA

http://pubs.acs.org/journal/acsodf

Article

Topological Impact of Delocalization on the Stability and Band Gap of Partially Oxidized Graphene

Gaurav Jhaa, Pattath D. Pancharatna, and Musiri M. Balakrishnarajan*

Cite This: *ACS Omega* 2023, 8, 5124−5135

Read Online

ACCESS | Metrics & More | Article Recommendations | Supporting Information

ABSTRACT: Strategic perturbations on the graphene framework to inflict a tunable energy band gap promises intelligent electronics that are smaller, faster, flexible, and much more efficient than silicon. Despite different chemical schemes, a clear scalable strategy for micromanaging the band gap is lagging. Since conductivity arises from the delocalized π-electrons, chemical intuition suggests that selective saturation of some sp^2 carbons will allow strategic control over the band gap. However, the logical cognition of different 2D π-delocalization topologies is complex. Their impact on the thermodynamic stability and band gap remains unknown. Using partially oxidized graphene with its facile and reversible epoxides, we show that delocalization overwhelmingly influences the nature of the frontier bands. Organic electronic effects like hyperconjugation, conjugation, aromaticity, etc. can be used effectively to understand the impact of delocalization. By keeping a constant C_4O stoichiometry, the relative stability of various π-delocalization topologies is directly assessed without resorting to resonance energy concepts. Our results demonstrate that >C═C< and aromatic sextets are the two fundamental blocks resulting in a large band gap in isolation. Extending the delocalization across these units will increase the stability at the expense of the band gap. The band gap is directly related to the extent of bond alternation within the π-framework, with forced single/double bonds causing the large gap. Furthermore, it also establishes the ground rules for the thermodynamic stability associated with the π-delocalization in 2D systems. We anticipate that our findings will provide the heuristic guidance for designing partially saturated graphene with the desired band gap and stability using chemical intuition.

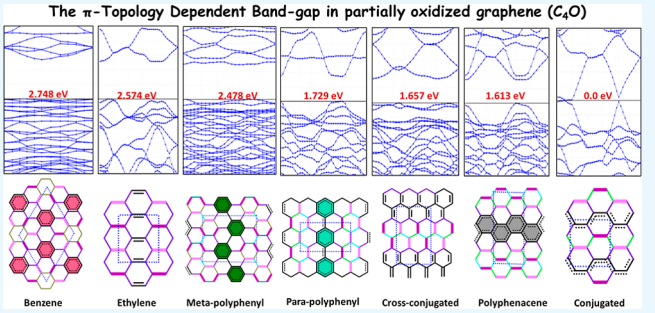

1. INTRODUCTION

Delocalization is a prequantum construct that is a cornerstone of chemical bonding theory.[1] It was postulated based on the axiomatic existence of atoms and bonds in the chemical description of matter and expectedly evaded universally acceptable definitions.[2] After the advent of modern atomic theory, delocalization became a chemical precept linked to the fictitious movement of electrons.[3] Typically drawn with dotted lines, it is also often shown with curved arrows indicating the direction of movement between representative Lewis structures. However, it is not related to the actual movement of electrons or observable in the strict quantum mechanical sense. Electrons being indistinguishable fermions move in mysterious ways, and the uncertainty principle forbids its tracking. Despite its contrived basis, delocalization remains a powerful paradigm in the ontology of covalent bonding, particularly in organic chemistry.

Among the quantum mechanical models of chemical bonding, valence band (VB) theory allows its exposition through resonating Lewis structures. The resonance theory of electrons has evolved successfully in the classical description of various electronic effects, ring currents, and reaction trajectories from the representative chemical structure by the arrow-pushing mechanism. As a stabilizing phenomenon, the extent of delocalization depends qualitatively on the energetic proximity of the resonance structures in VB theory.[4] Intriguingly, in molecular orbital (MO) theory, where all electrons occupy MOs that are inherently delocalized over several atoms, delocalization is understood qualitatively from the mixing and the avoided crossings of wavefunctions from the virtual to occupied space[5] and is typically studied from the interaction of the fragment orbitals. Here, delocalization depends on the energetic proximity and overlap between the frontier MOs involved in second-order mixing and thus offers a handle for tuning the highest occupied MO (HOMO)−lowest unoccupied MO (LUMO) gap. The π-type interactions facilitate delocalization since their poor lateral overlap leads to narrow splitting of levels that effectuate mixing.

The intrinsic attributes of valence AOs of carbon, that is, their relative energies and size, are optimal for the persistent

Received: December 24, 2022
Accepted: January 13, 2023
Published: January 26, 2023

domination of π-type interactions in the frontier[6] and increase the importance of delocalization in organic systems. Hence, engineering the band gap for two-dimensional (2D) nanosheets by chemical intuition is easier for planar networks based on delocalized sp^2 carbon due to the total domination of π-electrons in their Fermi surface. Despite the $\sigma-\pi$ inseparability of the Hamiltonian, the symmetric contradistinction of π-bands from the σ-framework due to network planarity offers easier cognition of the avoided crossings in the frontier bands. Though π-bonds are weak, delocalization stabilizes the sp^2 carbon network, which is evidenced in its allotropes[7] and argues for the high thermodynamic stability of these nanosheets. Electronic effects from the delocalization of π-electrons are described as conjugation, aromaticity, etc. in organic chemistry and hold the key to band gap engineering. However, there are inherent complexities in quantifying these effects.[8]

Among the possible network topologies based on sp^2 carbon, the π-delocalization in the linear chains is well-described by conjugation through the arrow-pushing mechanism in its Lewis structure with alternating single and double bonds. Linear conjugation of these double bonds is stabilizing, making them less reactive, albeit at the expense of the HOMO−LUMO gap. However, cyclic conjugation is not always stabilizing as implied by the resonance theory and necessitates the MO approach, like Hückel, to explain the nature of the ground state. Hückel's method helped deduce the empirical $4n+2$ rule for aromatic stability in monocyclic systems. Aromatic π-delocalization in cyclic conjugated hexagonal rings, represented with an inscribed circle, exhibits exceptional stability without compromising the HOMO−LUMO gap at the Hückel level, unlike linear conjugation. Unfortunately, the $4n+2$ rule is not applicable in extended delocalization involving polycyclic systems. They exhibit many Kekulé resonance structures, making it impossible to represent the chemical structure uniquely.

The aromatic sextet is the preferred motif for extended hexagonal networks when these localized aromatic sextets are in conjugation.[9] Since hexagonal geometry is ideally suited for sp^2-hybridized carbon, atomistically thin graphene, with its semimetallic hexagonal network and high thermodynamic stability, conceptually provides an ideal canvas for design strategies to engineer the band gap.[10,11] Synthesizing a tunable band gap in semimetallic graphene requires prudent control of π-electron delocalization. Approaches based on quantum interference[12] and confinement[13] lead to the development of nanoribbons, nanodots, nanoflakes, nanomesh, etc. Though these open the band gap, they suffer from the excessive sensitivity of frontier bands by the nature of truncated edges. Functionalization using the chemical rationale may help fine-tune the nature and magnitude of the gap required for various electronic, optical, and catalytic applications. With the advent of atomic layer deposition (ALD) processes[14,15] that help engineer nanoscale chemisorption and desorption, tactful disruption of π-electron delocalization by saturating a few sp^2 carbon atoms appears to be more promising.

Among the various strategies, selective conversion of carbon hybridization from sp^2 to sp^3 is explored mainly through oxygen due to the facile and reversible epoxidation process. Several theoretical and experimental studies have been conducted on band gap openings in partially oxidized graphene.[16−18] Most of them attribute the magnitude of the band gap to the degree of oxidation, overlooking the π-topology despite the domination of π-type interactions in the frontier.[19] The possibility of a slew of variations in topological pathways entails combinatorial growth of isomeric possibilities for epoxide distribution. Though it poses dire modeling problems, it also offers many ways to fine-tune the band gap. However, there is a lack of fundamental understanding of the relative kinetic and thermodynamic stabilities of various delocalization topologies and their impact on the band gap. The steric repulsion between the lone pairs of proximate oxygen atoms is the dominant factor affecting the stability in completely oxidized graphene.[20] Some experimental studies and density functional theory (DFT) calculations point to the tendency for segregation of epoxide groups from the delocalized π-bonding in partial oxidation processes.[16−19]

The semimetallic nature of the graphene arises from the delocalization of π-electrons evenly across all the three symmetrically equivalent bonds of sp^2 carbon. Hence, we attempt to create an imbalance by partial saturation of sp^2 carbon atoms through epoxidation. Beginning with the completely isolated >C═C< double bonds by epoxides, we incrementally increase the extent of π-delocalization to the conjugated and aromatic lattices in various topologies to study their impact on the band gap. To assess the relative thermodynamic stability across different systems, we fixed the stoichiometry to C_4O, which balances the sp^2 and sp^3 carbon atoms. Epoxides can be prudently distributed to minimize the steric repulsion from the oxygen lone pairs as it is the prime factor that dominates the energetics of the interaction between epoxides. Epoxidation is also ideal for minimizing the impact on π-delocalization due to the conformational rigidity and perseverance of planarity of the underlying carbon framework to a large extent, despite having sp^3 carbon atoms. The energetics of epoxide distribution in partially oxidized graphene may also shed light on the mechanistic information related to memristors based on partially oxidized graphene.[21−24] This missing fourth fundamental nonlinear circuit element[25] has the promise to revolutionize nanoelectronic memory devices, computer logic, and neuromimetic architectures.

2. RESEARCH METHODOLOGY

We employed molecular models with and without hexagonal constraints to study the nature of the interaction among epoxides, >C═C< groups, and their combinations. Geometry optimization and characterization of stationary points for molecules are performed at the standard CCSD/aug-cc-pVTZ//B3LYP/6-311G(d,p) levels using the Gaussian 09 package.[25] Periodic DFT calculations on the C_4O sheets are performed via plane-wave pseudopotential methods using the Cambridge Ab Initio Serial Total Energy Package (CASTEP)[26] program. Due to a vast number of isomers with large unit cells, we primarily used the Perdew−Burke−Ernzerhof (PBE)[27] functional in nonlocal corrected generalized gradient approximation (GGA),[28] including Grimme's dispersion correction to account for weak interactions between oxygen lone pairs. These are primarily used to compare the optimized geometries, energies, and band structures. The trends in energetics remain largely unaltered even if simple local density approximation (LDA)[29] with CA-PZ (Ceperley and Alder data as parametrized by Perdew and Zunger)[30] is used. However, all the bond lengths are uniformly elongated in GGA. We employed the ultrasoft pseudopotential with a plane-wave basis with a kinetic energy cutoff of 600 eV in a

https://doi.org/10.1021/acsomega.2c08169
ACS Omega 2023, 8, 5124−5135

Monkhorst−Pack[31] mesh with 0.04 1/Å separation in the two lattice directions for all the calculations. The adjacent sheets are kept 20 Å away to avoid all possible interactions. Individual atom positions and lattice parameters were simultaneously optimized for self consistent field (SCF) tolerance (5.0×10^{-6} eV/atom) and forces (0.01 eV/Å) to arrive at the well-converged geometries. For phonon dispersion, the same dispersion-corrected GGA formulation is employed but with norm-conserving pseudopotentials using the linear response method and Koelling−Harmon relativistic treatment. All the nanosheets are kinetically stable except for some aberrations near the gamma for acoustic phonons, which are presumably interpolation artifacts. The bond lengths are uniformly elongated with norm-conserving pseudopotentials. Atom and orbital projected density of states (DOS) values from DFT and extended Hückel calculations are employed for mapping the frontier bands to fragment orbitals that help in understanding the nature and magnitude of band gaps. The extended Hückel[32] (eH) calculations were performed using CACAO[33] and YAeHMOP packages.

Mapping fragment MOs to bands is needed to deduce design rules for band gap engineering as it is proven effective in understanding electronic effects in 2D nanosheets.[34,35] Besides, we correlate the DFT band structure and energies with tools in chemical graph theory that estimates resonance energy or aromaticity of polycyclic benzenoid hydrocarbons. The extent of delocalization is measured popularly with the number and nature of VB-type Kekulé resonance structures[36] as they contribute significantly to the ground state and correlate with resonance energy. With few exceptions,[5] graph theoretic reports do not appraise the nature of the frontier or extend readily to periodic systems. Delocalization and its relationship with physical observables are the challenges in two dimensions.[37] We anticipated that their qualitative stability description may correlate with the band gap and help the system design.

3. RESULTS AND DISCUSSION

We restricted ourselves to partially oxidized graphene nanosheets that exclusively have epoxides and >C═C< double bonds, leaving the reactive radical centers out of the current inquiry. The constant stoichiometry C_4O has equal amounts of epoxides and double bonds on the graphene lattice with varying topologies and allows direct comparison across distinct networks. Beforehand, we probed the nature of interactions between epoxides and >C═C< groups using molecular models to understand their stability and the HOMO−LUMO gap comprehensively.

3.1. Conjugation versus Hyperconjugation in Molecular Models. We probed the three distinct junctions involving epoxides and double bonds possible, inspecting the nature of electronic effects. The change in the optimized geometry in the most stable s-*trans* isomers (Figure 1) reflects the impact of delocalization.

Though the central C−C bond in the epoxy dimer (Figure 1a) is shortened (<1.5 Å), the C−O bond hardly shows any elongation (0.004 Å) compared to oxirane (1.429 Å), indicating negligible hyperconjugation. This rules out the suspected partial π-bonding of the central C−C bond (donation of C−O σ to C−O σ^*), and its shortening is largely due to the bent nature of the exo-2c-2e bonds of the strained triangular ring.[20] In the epoxide−double bond junction (Figure 1b), the proximate C−O bond elongates by

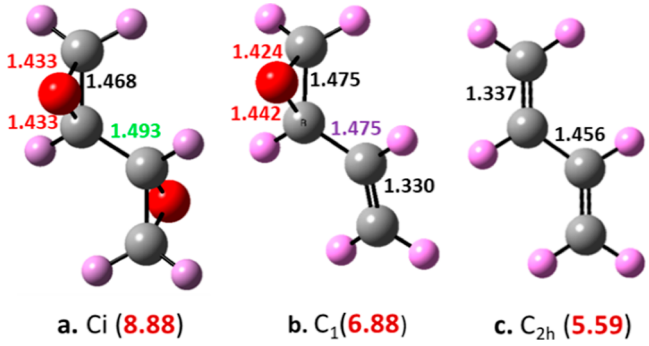

Figure 1. DFT optimized geometries of (a) epoxide dimer, (b) epoxide and >C═C< double bond, and (c) s-*trans*-butadiene. The computed HOMO−LUMO gap is given within braces.

0.013 Å, implying a tangible increase in the π-delocalization, shortening the central C−C bond further. The delocalization is significantly more in butadiene (Figure 1c) where the central C−C bond is substantially shortened by π-conjugation.

The observed HOMO−LUMO gap of these molecular models correlates well with the geometrical variations. The HOMO of epoxide is a p-type oxygen lone pair with little mixing from carbon atoms. However, the low symmetry of these systems allows the mixing of the sp- and p-type lone pairs with C−O σ-bonding MOs in these molecules (Figure 2) and the nanosheets.

The epoxide dimer has the highest gap, which is only slightly lower than that of the monomer due to insignificant hyperconjugative delocalization since the donation of C−O σ to C−O σ^* orbitals is very weak. The energy mismatch between them is a direct consequence of the large HOMO−LUMO gap of the epoxide. On the other hand, >C═C< groups exert appreciable delocalization due to the low-lying C−C π-antibonding leading to the significant reduction in the HOMO−LUMO gap of the composite molecules. The HOMO−LUMO gap reduces further in butadiene due to conjugation. Overall, all the composite systems have reduced HOMO−LUMO gaps compared to their monomers due to delocalization to varying degrees.

Interactions of epoxides and >C═C< groups within the hexagonal constraint effectuate large variations in the HOMO−LUMO gaps. We probe two isomeric models with two double bonds within a hexagonal ring and two exoepoxides, which are isoenergetic (<1 kcal/mol) and optimized geometries (Figure 3) that show subtle variations in the bond lengths and HOMO−LUMO gap. Though there are other isomeric possibilities, they are higher in energy.

Hyperconjugation leads to the elongation of the proximate C−O bonds (lateral splaying). It is enhanced with the two >C═C< groups in 3a and becomes comparable to the impact of conjugative stabilization in 3b. The increased hyperconjugative stabilization in 3a is due to the planarity of the carbon network, where each sp^3 carbon is incident to two >C═C< groups enabling "through bond" interaction between double bonds. This topology allows definite cyclic π-delocalization in the hexagonal ring, resulting in pseudoaromaticity. The out-of-plane distortion forced in 3b by the gauche effect between epoxides reduces the π-overlap between conjugated double bonds, making it comparable to the hyperconjugative impact on 3a. However, the enhanced delocalization from conjugated double bonds reduces its HOMO−LUMO gap substantially compared to that of 3a, in

https://doi.org/10.1021/acsomega.2c08169
ACS Omega 2023, 8, 5124−5135

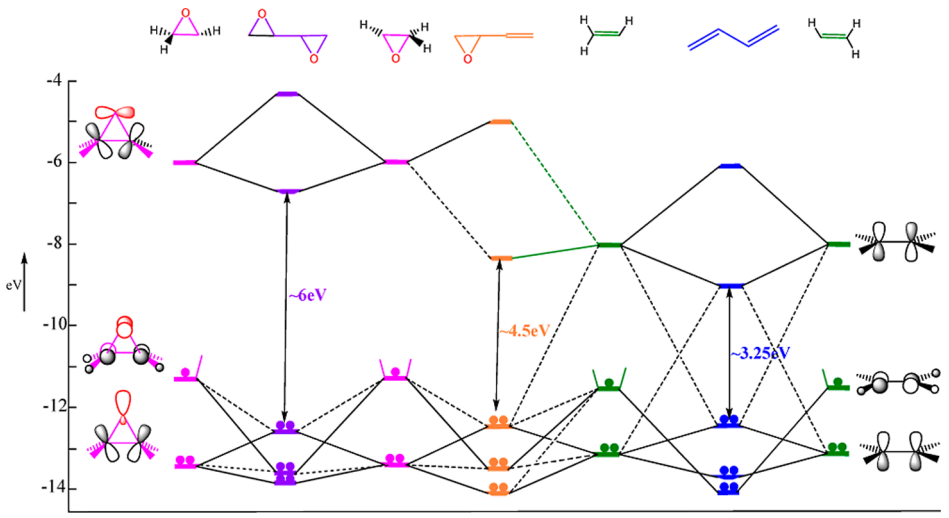

Figure 2. eH-based interaction−correlation diagram of the epoxide dimer (right), epoxide with >C═C< (middle), and butadiene (right) showing the variation in the HOMO−LUMO gap. The dotted lines indicate higher-order mixing.

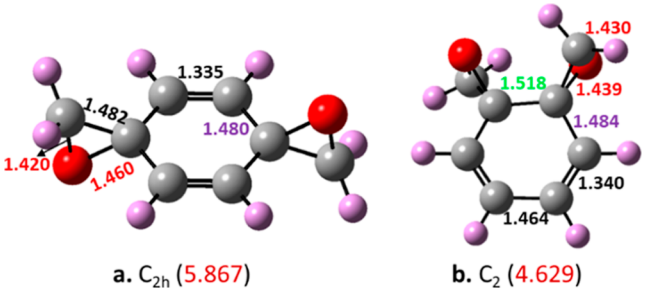

Figure 3. DFT optimized geometries of diepoxy derivatives of (a) 1,4-cyclohexadiene and (b) 1,3-cyclohexadiene. The computed HOMO−LUMO gap is given within braces.

which pseudoaromatic interactions arise from hyperconjugation.

A similar effect is reported with cyclohexadiene isomers,[38] where 1,4-diene exhibits swapping of its frontier π-MOs in both occupied and virtual space[39] (see Section S5, Supporting Information). The impact of conjugation and hyperconjugation in different topologies has a subtle effect on delocalization. Though both are stabilizing, the band gap is substantially reduced by π-conjugation.

3.2. Topological Variations in C_4O Nanosheets. The bonding variations in molecular models provide pivotal guidance for designing isomers of C_4O nanosheets with varying band gaps since delocalization effects like aromaticity, conjugation, hyperconjugation, etc. play a vital role. The steric repulsion between oxygen lone pairs that is detrimental to the stability can be partially offset by lateral splaying that leads to nonequivalent C−O bonds within the epoxide ring or orthogonal axial splaying.[20] Assuming that π-delocalization reduces the band gap, epoxides are distributed prudently on the graphene lattice to vary the topology of π-delocalization. Epoxides are distributed on either side of the graphene surface to minimize the steric repulsion between oxygen lone pairs. Lattices with symmetrically equivalent epoxides are selected to keep the size of the unit cell manageable, except when it is impossible to have a desired delocalization topology. We start with the isolated π-bonds and progressively extend the delocalization to probe its impact on the stability and nature of the band gap. The 2D lattice symmetry is assigned by treating the epoxides on different sides as distinct.

3.2.1. Isolated π-Bonds. The isomer having periodic alternation of >C═C< bonds and epoxides along both armchair and zig-zag directions (Figure 4a) has a rectangular lattice having two formula units (Z = 2) of C_4O, with two distinct Csp^3−Csp^2 interactions, *intra* (within the same ring) and inter (across adjacent rings). On optimization, *intra* is marginally longer than *inter* due to the slight variation in the hyperconjugative delocalization involving the donation of C−O σ to C−C π^* orbitals (Figure 4b). The >C═C< π-bonds

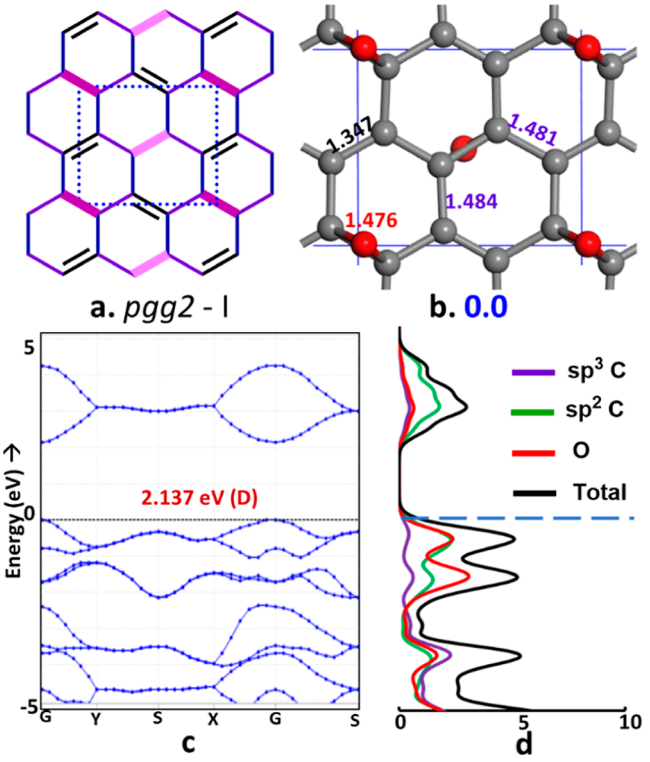

Figure 4. C_4O sheet having isolated double bonds distributed one per hexagon: (a) 2D lattice symmetry, (b) optimized geometry, (c) band structure, and (d) atom-projected DOS.

https://doi.org/10.1021/acsomega.2c08169
ACS Omega 2023, 8, 5124−5135

and oxygen lone pairs dominate the top two valence bands. They split at the gamma but remain degenerate at other symmetry points of the Brillouin zone, indicating negligible communication across π-electrons (Figure 4c).

The C−O σ-orbitals lie low, stabilized by hyperconjugative mixing from >C═C< π^*-orbitals as indicated by the oxygen-projected DOS. There is hardly any interaction between them, leading to minor splitting. The conduction band is dominated by the two >C−C< π^* orbitals, pushed up by hyperconjugation, and split only at the gamma, leading to the direct band gap. We use this nanosheet as the reference to compare the stability (in kcal/mol per C_4O unit) of other isomers. Its Janus isomer having all the epoxides on the same side of the graphene surface has a similar electronic structure with a marginal reduction in the band gap (2.116 eV). They are comparable in energy (<1 kcal/mol) as oxygen atoms are far separated to exert any steric problems.

An alternate distribution of isolated >C═C< bonds is to align them along the armchair direction, resulting in a 1,4-cyclohexadiene motif (Figure 5a). This lattice (Z = 2) forces all

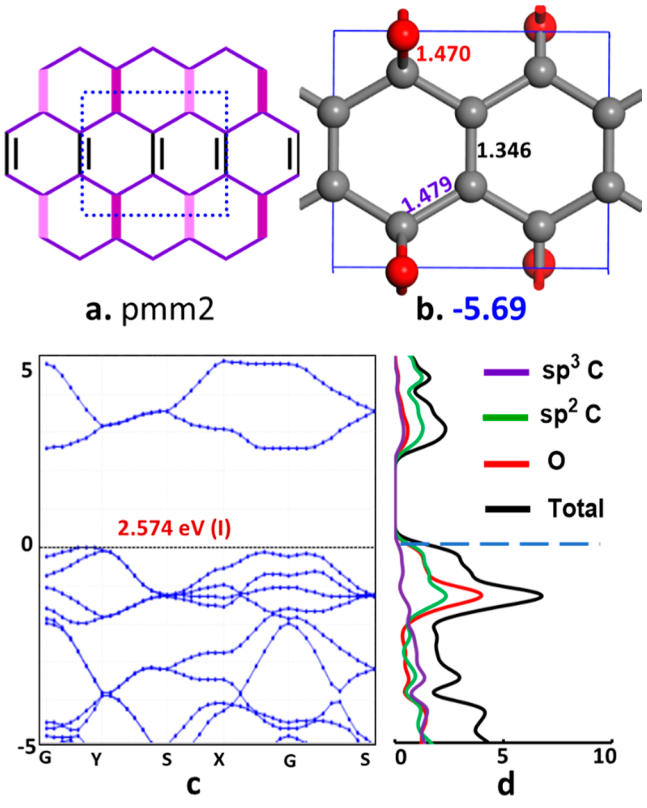

Figure 5. C_4O nanosheet having isolated double bonds with the 1,4-cyclohexadiene motif: (a) 2D lattice symmetry, (b) optimized geometry, (c) band structure, and (d) atom-projected DOS.

the Csp^3−Csp^2 interactions to be symmetrically equivalent. Hyperconjugation shortens these bonds (Figure 5b), but the increase in C−O distances is moderate. Unlike *pgg2-I* (Figure 4), hyperconjugation also mediates "*through bond*" interactions, leading to pseudoaromaticity within the ring. The topology extends delocalization across these pseudoaromatic rings by edge sharing, which increases its stability unlike the molecule (Figure 3a). The split-off between the π-dominant valence bands from the σ-framework vanishes since the enhanced delocalization from hyperconjugation increases the width. Besides, lattice symmetry forces additional degeneracy at S. This increased width of the valence π-bands shares the same energy window with the oxygen lone pair (Figure 5c) as seen from the oxygen-projected DOS (Figure 5d).

As seen in the molecular model (Figure 3a), the mixing of C−O σ-MOs happens only with one of the π^* Mos, the one with the in-phase combination of the two π-antibonding fragments MOs of the 1,4-cyclohexadiene unit (see S5, Supporting Information). Similar mixing pushes the conduction bands further up, resulting in a larger band gap despite the pronounced delocalization. The conduction band minimum is at the gamma, but the valence band maximum is shifted slightly, leading to an indirect band gap presumably due to the "through bond" interactions between *intra* π-bonds.

Its Janus isomer[19,40] is less stable than *pgg2*-I by 2.45 kcal/mol and shows a reduced gap of 1.702 eV, which is presumably due to steric repulsion from p-type oxygen lone pairs. Compared to *pgg2-I*, the 1,4 cyclohexadiene motif has an increased band gap due to the pseudoaromaticity arising from through−bond interactions.

3.2.2. Conjugated Systems. We start with the lattice having restricted conjugation along the armchair direction. It is constructed from one-dimensional (1D) carbon chains with a periodic alternation of two conjugated double bonds (s-*cis* butadiene motif) and two epoxide groups (intra-*trans*). Juxtaposing these chains in the second dimension leads to a rectangular lattice (Z = 4) with alternating epoxides and double bonds in the zig-zag direction (Figure 6). Here, for every Csp^2−Csp^2 single bond stabilized by conjugation, there are three hyperconjugative interactions stabilizing the three discrete Csp^3−Csp^2 single bonds.

The bond length variations in the formal C−C single bonds of the representative resonance structure perfectly reflect the extent of delocalization. Bonds connecting epoxide groups to

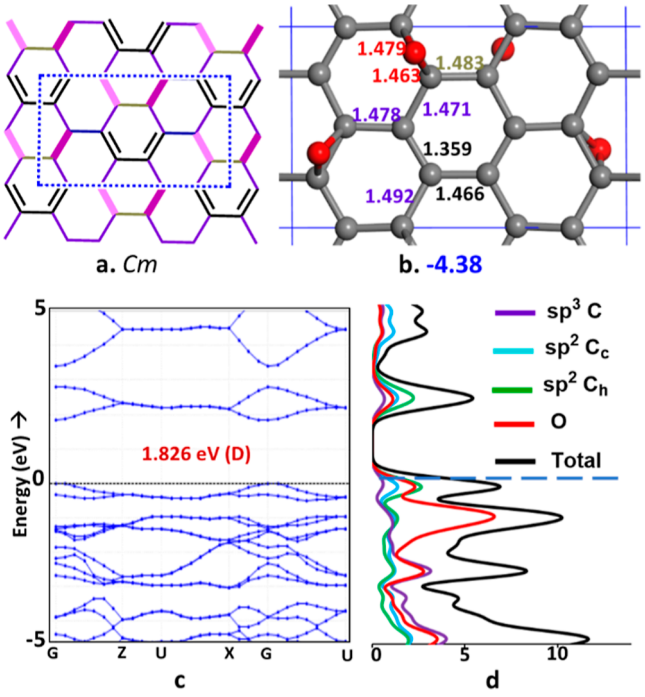

Figure 6. C_4O sheet having conjugated double bonds with s-cis butadiene motif: (a) 2D lattice symmetry, (b) optimized geometry, (c) band structure, and (d) atom-projected DOS.

https://doi.org/10.1021/acsomega.2c08169
ACS Omega 2023, 8, 5124−5135

the central carbons of the butadiene fragment are the longest due to the reduced hyperconjugation arising from the smaller size of its coefficients in the LUMO of the butadiene fragment. The next longest is the interepoxide junction with negligible hyperconjugation but bond bending. The epoxide junctions having *intra*- and *inter*-type hyperconjugation with the terminal carbon atoms of the butadiene fragment appear next in that order. The shortest is the central bond of the butadiene unit due to π-conjugation. The reduced symmetry of the lattice allows lateral oxygen splaying. The presence of π-conjugation effectively reduces the gap, making it more stable than the reference *pgg2-I*.

Despite π-conjugation, this isomer is less stable than *pmm2* (Figure 5a) with isolated double bonds. This indicates that the conjugative stabilization is less pronounced than the pseudoaromatic hyperconjugation arising from the planarity of the 1,4 cyclohexadiene fragment. The frontier bands map perfectly with the butadiene frontier MOs and appear in pairs due to the duo of butadiene fragments in the cell. They have a minor splitting at the gamma, leading to a direct gap. The projected DOS shows significant oxygen mixing, indicative of definite hyperconjugation. Its reduced strength results in flat valence bands splitting off from the rest. The Janus isomer[19] of this sheet has a direct gap (1.38 eV) and is less stable by 8.67 kcal/mol.

The lattice hosting the *trans*-butadiene motif (Figure 7) is constructed by starting with a linear chain of alternating

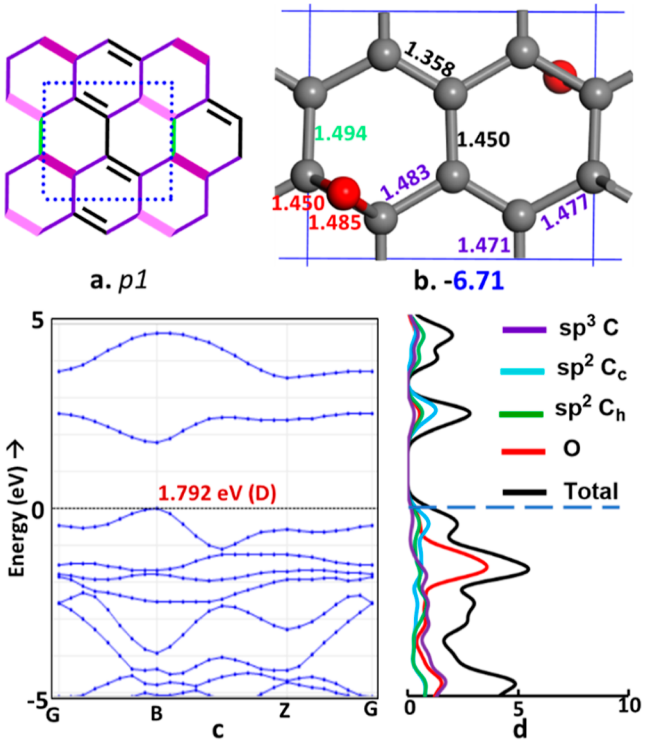

Figure 7. C_4O sheet having conjugated double bonds with the *trans*-butadiene motif: (a) 2D lattice symmetry, (b) optimized geometry, (c) band structure, and (d) atom-projected DOS.

epoxide and >C═C< units in the zig-zag direction as in *pgg2-I* but linking these parallel chains with an alternate stacking that curtails conjugation to two double bonds ($Z = 2$).

The length of conjugation can be controlled by manipulating the stacking of these 1D chains. Increased conjugative delocalization in this isomer is reflected in the reduced bond alternation (0.092 Å) in the butadiene unit. In addition, the pronounced hyperconjugative stabilization arising from the pseudoaromaticity of the planar 1,4-hexadiene fragment and the lack of steric repulsion between the epoxides aided by the network topology makes this isomer substantially more stable than its *cis* counterpart (*Cm*) by 2.5 kcal/mol.

The optimized bond lengths precisely show the cause of the underlying electronic effects. The band structure has a split-off valence band with a larger width, reflecting the increased delocalization and the subsequent reduction in the band gap. The minimal oxygen projected DOS in the frontier reflects the domination of >C═C< units in conjugation.

Increasing the conjugation length is expected to progressively increase the stability while reducing the band gap. However, extending the conjugation to infinity may also lead to Peierls distortion[41] as in conjugated polymers.[42] To probe this impact, we constructed two C_4O nanosheets with infinite conjugation in the orthogonal (zig-zag and armchair) directions. The sheet having infinitely extended conjugation in the zig-zag direction when interspersed with alternating epoxide chains has an oblique unit cell ($Z = 2$). The reduction in symmetry due to the inter-*trans* orientation of epoxides naturally allows >C═C< bonds to localize if energetically favored (Figure 8). The optimized unit cell has a finite bond

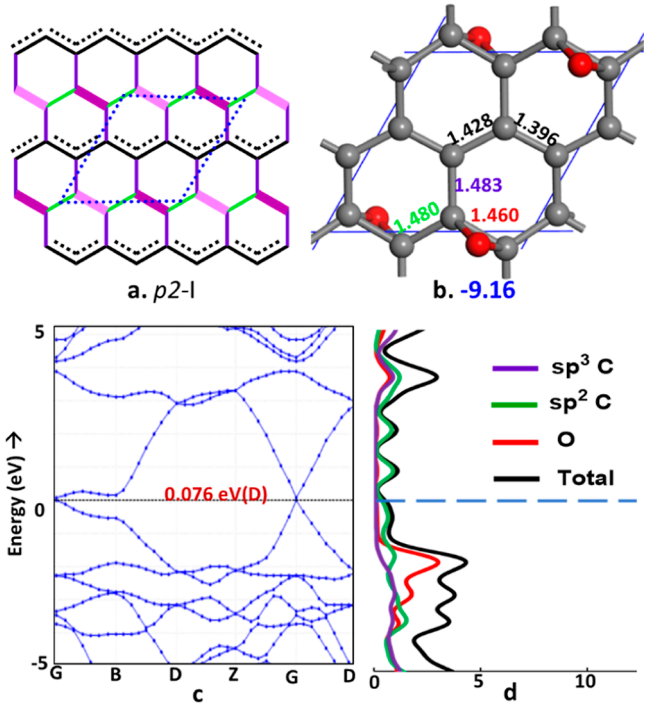

Figure 8. C_4O sheet having extended conjugation in one dimension with the *trans*-polyacetylene motif: (a) 2D lattice symmetry, (b) optimized geometry, (c) band structure, and (d) atom-projected DOS.

alternation (0.032 Å) between the C−C distances of the sp^2 carbon, much less than that of polyacetylene (0.08 Å). In addition to conjugation, hyperconjugation contributes significantly, increasing its stability as reflected in the bond lengths.

The reduction in bond alternation leads to a negligible band gap. The projected DOS shows substantial mixing of oxygen in the lower occupied π-band. Its Janus isomer is less stable by 12

https://doi.org/10.1021/acsomega.2c08169
ACS Omega 2023, 8, 5124−5135

kcal/mol due to the steric repulsion from oxygen atoms as they lie too close (<2.5 Å) and are forbidden from splaying due to symmetric constraints. However, it shows a significant band gap (0.348 eV).

The isomer with extended conjugation in the armchair direction forms a rectangular lattice (Z = 2) similar to *cis*-polyacetylene and allows localization of π-bonding (Figure 9).

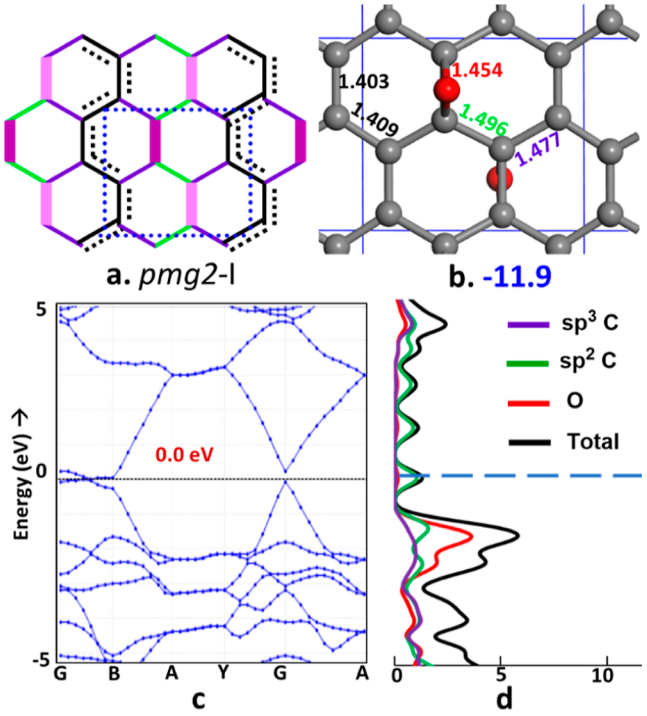

Figure 9. C_4O sheet having extended conjugation in one dimension with the *cis* polyacetylene motif: (a) 2D lattice symmetry, (b) optimized geometry, (c) band structure, and (d) atom-projected DOS.

However, the optimized geometry shows only a minor bond alternation (0.006 Å) and increased conjugative delocalization. Surprisingly, this is substantially more stable (~2.74 kcal/mol) than the *p*2-I isomer despite having similar interepoxide interactions. This trend is quite the opposite of the observations in polyacetylene isomers or even in the *cis*−*trans* isomers of butadiene-based C_4O sheets discussed earlier. The exceptional stability of this cisoid isomer and the negligible bond alternation along the sp^2 chain arise not just from the increased hyperconjugative interactions as seen in the reduced Csp^3-Csp^2 distances. Through hyperconjugation, the *cis*-butadiene units acquire additional stability through cyclic delocalization across the epoxide C−C bond. As part of the hexagonal ring, epoxide forces planarity, thereby effectuating pseudoaromatic stability, which is absent in the *cis*-butadiene-based isomer (*Cm*) or *cis*-polyacetylene. It has a metallic band structure expected from the lack of bond alternation. The frontier π-bands span a width of more than 5 eV. The lower occupied π-band shows mixing with oxygen and remains flat except at the gamma.

The final variation in acyclic π-delocalization is cross conjugation, which is the focus of active research in organic electronics.[43,44] The lattice with extended cross conjugation is constructed by stacking two layers of isolated double bonds that run perpendicular to the zig-zag direction (Figure 10).

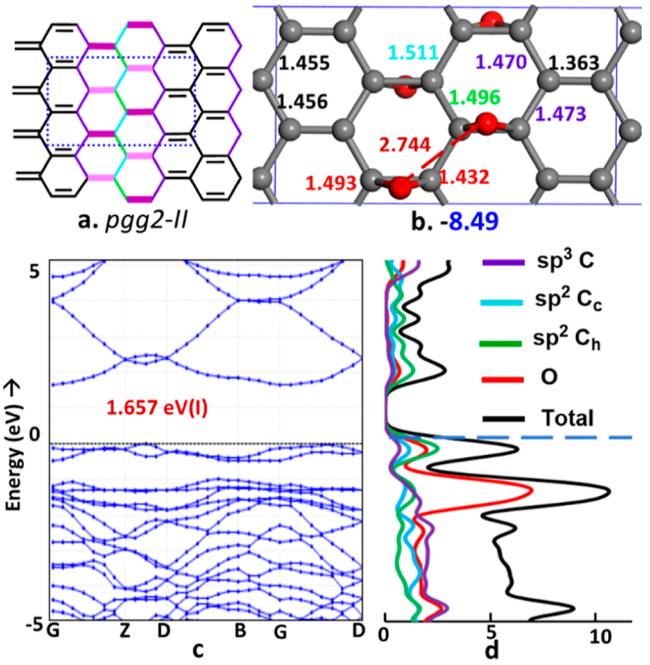

Figure 10. C_4O nanosheet having extended cross conjugation in one dimension: (a) 2D lattice symmetry, (b) optimized geometry, (c) band structure, and (d) atom-projected DOS.

These are interspersed with two layers of epoxide that are placed similarly on the graphene lattice, forming a rectangular unit cell (Z = 4). Increasing the number of these layers will increase the length of cross conjugation, providing additional flexibility for band gap engineering.

The conjugative delocalization in the infinite chains studied earlier (*p*2-I and *pmg*2-I) allows two possible Kekulé resonance structures that are energetically close. In contrast, cross-conjugation allows only one representative Kekulé resonance structure even though it is extended infinitely in one direction. Since this implies forced double bonds and single bonds, chemical intuition suggests that this will lead to reduced delocalization. The optimized geometry indeed shows large variations (~0.1 Å) in the C−C bond lengths between sp^2 carbon atoms. The reduction in the delocalization results in a substantial band gap and reduced stability compared to that in the other two sheets with infinite conjugation. In the band structure, the top two valence bands are flat and split off from the rest, presumably due to dominant nonbonding π-interactions within the sp^2 layers. Their flatness and reduction in oxygen DOS indicate reduced delocalization across the layers.

3.2.3. Aromatic Systems. Cyclic delocalization involving hexagonal rings is well-known for its pronounced aromatic stability without compromising the HOMO−LUMO gap. These cyclic networks can be isolated or connected or share one or more edges to extend the delocalization. The topological impact of aromatic delocalization on the stability and band gap of the C_4O is systematically explored by increasing the complexity progressively.

The C_4O network with isolated benzenoid rings, separated by interspersing of epoxides, forms a hexagonal lattice (Figure 11). The unit cell (Z = 6) has benzenoid rings with a reduced local (D_{3d}) symmetry that allows bond alternation. The optimized geometry shows minor bond alternation (0.025 Å) within the benzenoid ring. The C−O bonds show lateral

https://doi.org/10.1021/acsomega.2c08169
ACS Omega 2023, 8, 5124−5135

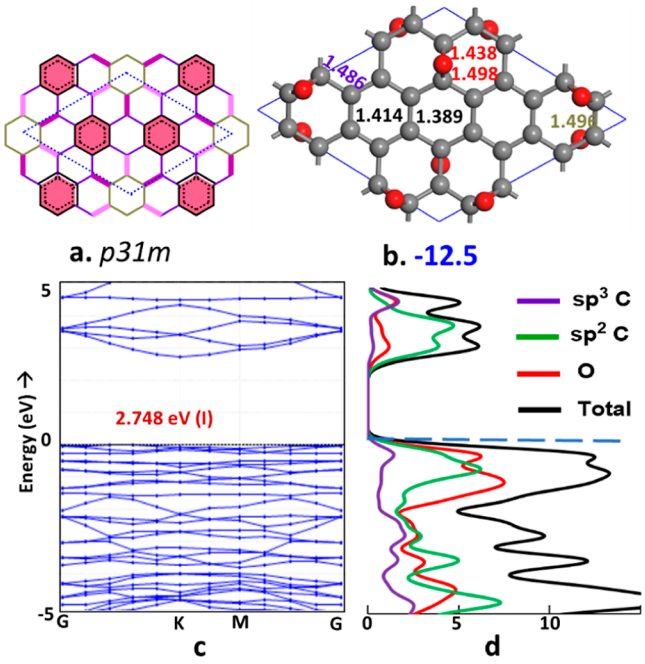

Figure 11. C_4O sheet having an isolated benzene motif: (a) 2D lattice symmetry, (b) optimized geometry, (c) band structure, and (d) atom-projected DOS.

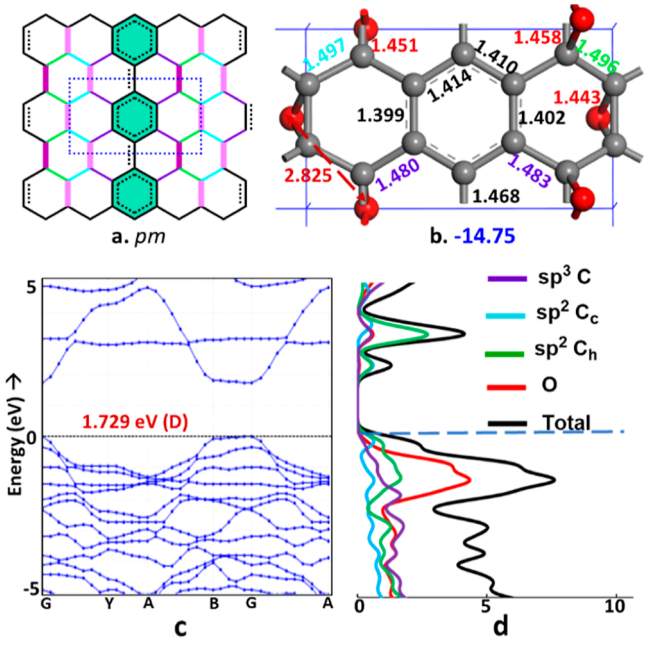

Figure 12. C_4O nanosheet having extended conjugation across benzene rings with the planar poly(*p*-phenylene) motif: (a) 2D lattice, (b) optimized geometry, (c) band structure, and (d) atom-projected DOS.

splaying, and one of the two epoxide C−O bonds elongates due to hyperconjugation. The aromatic delocalization within the benzenoid ring makes it more stable than all the acyclic conjugated systems discussed above. It also provides the largest band gap among all the C_4O isomers considered here. Compared to other acyclic π-delocalization systems, isolated aromatic rings provide more stability without compromising the HOMO−LUMO gap, as in the case of molecules.

The valence bands of π-electrons coalesce with the σ-bands and remain flat throughout the Brillouin zone, indicating reduced delocalization across unit cells. The atom-projected DOS of sp^2 carbon atoms lies below the oxygen, indicating excessive stabilization of the aromatic π-electrons, allowing the oxygen lone pairs to dominate the frontier. Nevertheless, the conduction bands are predominantly π-antibonding with some oxygen mixing. These observations also imply that an isolated benzenoid motif that forms localized Clar's sextets gives the largest gap between π-bands for a partially oxidized graphene oxide irrespective of the degree of oxidation. The band gap can be reduced by replacing the isolated benzene fragment with other benzenoid fragments of appropriate HOMO−LUMO gaps.

Next, the aromatic sextets are linked directly, promoting π-communication as in biphenyl. Extending them infinitely in one dimension gives two isomeric possibilities. The *para* network has the 1,4-connected benzenoid rings with interspersed epoxide chains forming a rectangular cell (Z = 3). This topology does not allow the ideal "all-*trans*" orientation across proximate epoxides. Hence, the next most favored inter-*cis* interaction is used to minimize the steric repulsion between the oxygen lone pairs (Figure 12).

The optimized geometry shows a shortening of the C−C bond linking the benzenoid rings, indicating a significant π-delocalization. Compared to the standard aromatic C−C bond length, the ring C−C bonds are slightly elongated (<0.02 Å) and also show mild bond alternation (~0.01 Å). The different epoxide bridges exhibit mild axial splaying, allowed by the lowered symmetry. Compared to the *p31m* isomer having isolated sextets, the extended delocalization across the sextets here provides additional stabilization of 2.25 kcal/mol for this network and also reduces the band gap by ~1 eV. Extended delocalization allows the valence bands to span more than 1 eV width and lift the sp^2 carbon framework to the frontier, yielding a direct band gap at the gamma.

An alternate topology with the 1,3 linking of benzenoid rings leads to a metaconnected network.[45] The resulting nonlinearity forces the interspersing epoxides to accumulate within a hexagonal ring (Figure 13). Its rectangular unit cell (z = 6) has destabilizing 1,3 intra-*cis* interactions between epoxides that make the C−C bonds between the benzenoid rings into two distinct types. In the optimized geometry, these distances were comparable to that of the para-connected network. Hence, the reduced stability of this network compared to that of its para isomer (*pm*) appears to arise from the steric repulsion between the proximate oxygen lone pairs.

However, the computed band gap is found to be substantially larger (>0.7 eV) than that of the para isomer, indicating reduced delocalization between aromatic sextets, thus leading to flat bands. The projected DOS shows finite domination of π-bands in the frontier, subduing the oxygen lone pairs. Clearly, π-delocalization between aromatic sextets is reduced in the *meta*-network, partially contributing to the instability. It correlates with the reduced number of Kekulé resonance structures in the metaconnected network since the bonds connecting benzenoid rings are forced single bonds in all these structures. These bonds lack definite elongation, presumably due to the network constraints arising from the epoxide sublattice.

The substantial variation in topology with the benzenoid motif involves sharing of edges. The linear polyacene[46]-type network with an interspersed layer of epoxides forms a rectangular network (Z = 4). This lattice can also be viewed as

https://doi.org/10.1021/acsomega.2c08169
ACS Omega 2023, 8, 5124−5135

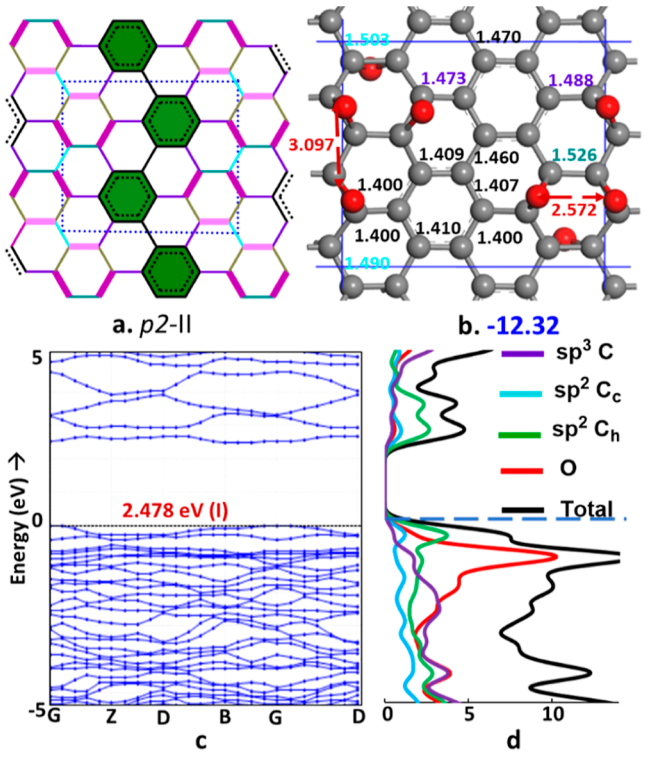

Figure 13. C_4O sheet with the planar poly(*m*-phenylene) motif: (a) 2D lattice, (b) optimized geometry, (c) band structure, and (d) atom-projected DOS.

a network that interlinks two infinite polyacetylene chains. The epoxides are effectively distributed on either side of the lattice to avoid steric repulsion, allowing bond alternation along the polyacetylene chains (Figure 14). The optimized geometry shows slight bond alternation of polyacetylene chains (0.003 Å) along the zig-zag direction, opening a smaller gap. However, the shared edges of the benzenoid rings are significantly longer, more in the range of Csp^3-Csp^2 distances. This disparity reduces the π-delocalization across the polyacetylene chains, which is detrimental to the stability.[47] Despite this shortcoming, the polyacene motif is more stable than the metaconnected *p2*-II benzenoid network but falls short of the para-connected *pm* isomer.

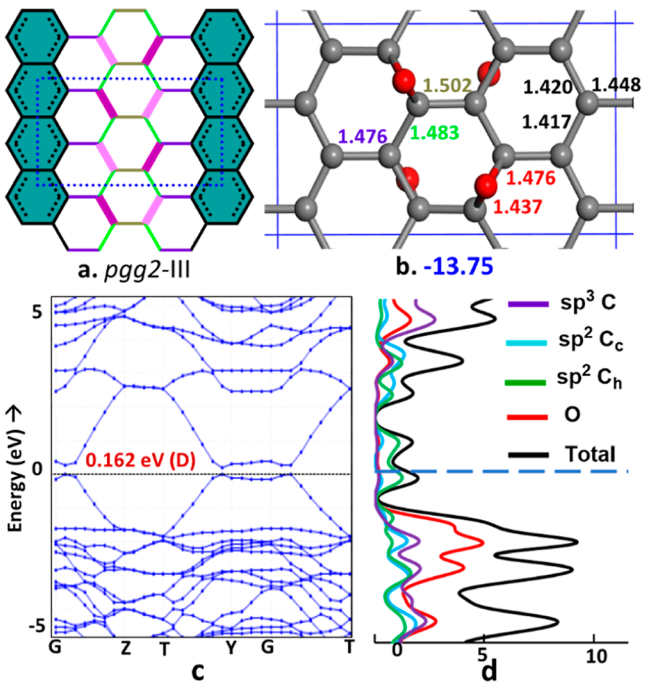

Figure 14. C_4O nanosheet having extended conjugation in one dimension with the polyacene motif with (a) 2D lattice symmetry, (b) optimized geometry, (c) band structure, and (d) atom-projected DOS.

The π-electrons dominate the frontier bands, and there is a small but definite direct band gap at the gamma, typical of polyacetylene rather than the benzenoid. The perceived loss of aromaticity is also observed in polyacenes.[48] The lack of aromatic stability originates from the impossibility of forming Clar's sextet, with the interchain bonds remaining single in all the possible Kekulé resonance structures. The sp^2 carbon linked to the epoxides dominated the DOS near the Fermi level and is presumably π-non-bonding.

The C_4O sheet with edge-sharing benzenoids can also have a phenacene[49] motif with interspersed epoxide layers running along the armchair direction. The topology of the resulting rectangular unit cell ($z = 4$) allows the distribution of epoxides with the favored inter-*cis* interactions (Figure 15). Compared

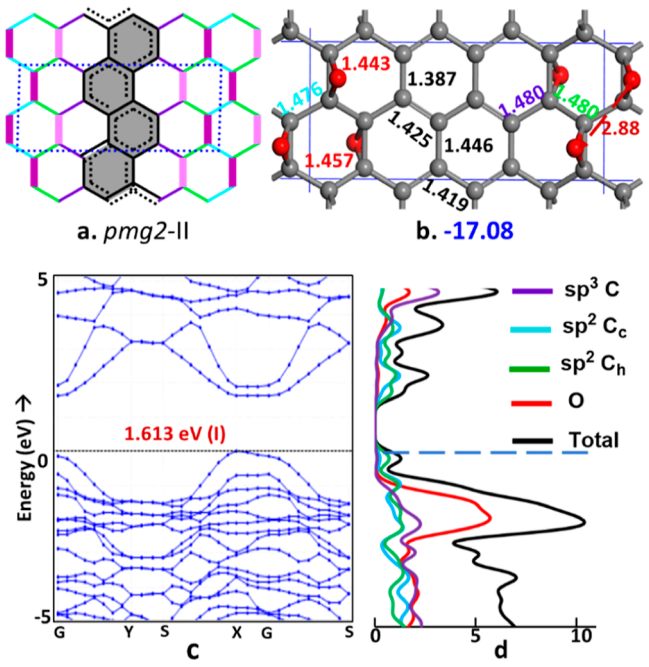

Figure 15. C_4O nanosheet having extended conjugation in one dimension with the polyphenacene motif: (a) 2D lattice symmetry, (b) optimized geometry, (c) band structure, and (d) atom-projected DOS.

to the acene isomer, the edges shared between the benzenoid units are shorter by 0.029 Å. In contrast, the bond connecting sp^2 carbon atoms incident to the epoxide units is shortened further, indicative of large π-character as in phenanthrene. These sp^2 carbon atoms dominate the frontier bands. Valence bands are π-bonding, and conduction bands are π-antibonding between them. There is a direct band gap at X along the phenacene chain.

The entire chain of benzenoids can also be visualized as an edge-sharing superposition of two *pm*-type chains of 1,4-connected Clar's sextets. The moderate bond alternation

https://doi.org/10.1021/acsomega.2c08169
ACS Omega 2023, 8, 5124−5135

within the sp^2 carbon sublattice without any forced double or single bonds results in increased π-delocalization with the attended reduction in the band gap and substantially increased stability. The increased stability also correlates with the increase in the number of Kekulé resonance structures, which increases the Shannon entropy of the information related to the distribution of double bonds.

3.2.4. sp^2 Networks Extended in the Second Dimension. Theoretically, one can extend the infinite 1D sp^2 network of acyclic and benzenoid motifs by stacking one or more layers laterally to increase the π-delocalization. All the networks having infinite 1D chains can be, in principle, extended. We extended the most stable network with the phenacene motif to assess its impact on its thermodynamic stability and band gap.

Stacking two layers of phenacene together by edge sharing leads to a rectangular unit cell ($Z = 6$). The symmetry remains the same (Figure 16), and the range of C−C distances between

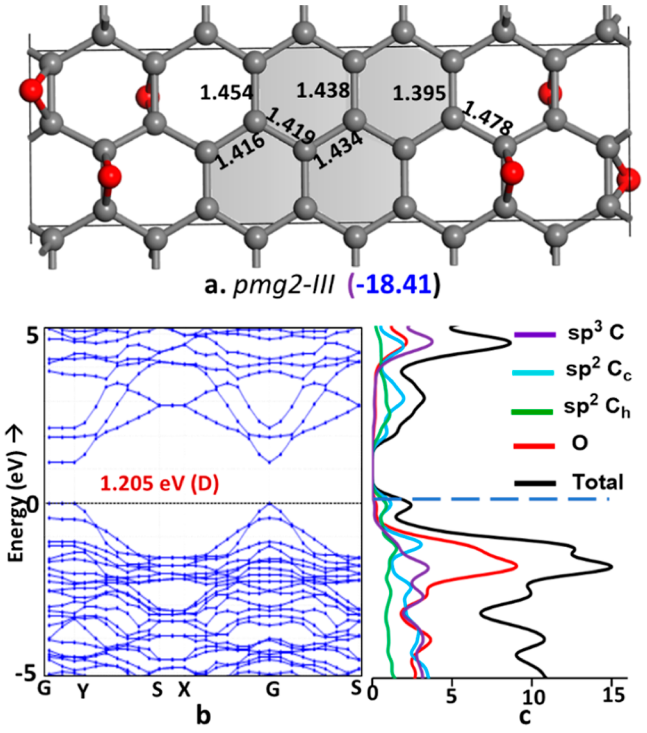

Figure 16. C_4O nanosheet having extended conjugation with a double-layered polyphenacene motif: (a) optimized geometry of the 2D lattice, (b) band structure, and (c) atom-projected DOS.

the sp^2 carbon atoms is narrowed, indicating larger delocalization. The additional layer increases its stability by 1.34 kcal/mol per C_4O unit. The inner sp^2 chain shows moderate bond alternation while more significant variations occur at the periphery of the aromatic framework. As expected, the frontier bands are dominated by sp^2 carbon atoms, presumably from π-type MOs that span a larger width than the single-layer phenacene nanosheets. As a result, there is a direct band gap at the gamma, with its magnitude reduced by ∼0.4 eV.

Further moderation of bond alternation within the sp^2 sublattice is observed in stacking one more layer of phenacene (see Section S3, Supporting Information, isomers 50 and 52). The stability increases by a meager ∼0.4 kcal/mol, but the band gap reduces drastically (<0.1 eV). Clearly, increasing the number of layers of phenacene will lead to metallicity with a slight gain in stability. Similar effects were observed in stacking other extended sp^2 networks (see Section S3, Supporting Information).

From these observations, we can deduce that the band gaps, if they exist, will reduce progressively and turn metallic with increased stacking. At the same time, energies improve modestly and converge to a constant value. Instead of stacking infinite 1D chains of sp^2 networks in the nanosheets, it is possible to have infinitely extended conjugation in two dimensions simultaneously. However, the size of such a network having C_4O stoichiometry is prohibitively large to be considered here.

4. CONCLUSIONS

The topological factors are proved effective for micro-engineering the band gaps and thermodynamic stabilities of partially oxidized graphene and can be rationalized using the electronic delocalization effects of organic chemistry. The primary stabilizing effects arise from the mixed blend of hyperconjugation, π-conjugation, and pseudoaromatic/aromatic delocalization within the benzenoid ring in increasing order barring a few exceptions. In their isolated existence, two distinct substructures, the >C═C< unit and the aromatic sextet, open the largest possible band gap in the partially oxidized graphene. Progressive extension of conjugation from these fundamental units will result in a proportional reduction in the band gap and a subsequent increase in their thermodynamic stability. Isolated molecular fragments of sp^2 carbons separated by sp^3 carbons of the epoxide groups will have the band gap mostly direct with its magnitude proportional to the HOMO−LUMO gap of corresponding conjugated hydrocarbon with a minor increase in the hyperconjugative effects. The band gaps of one-dimensionally extended conjugated systems mostly have indirect band gaps, whose magnitude is proportional to the degree of asymmetry in their π-bond order. Network topologies that allow fixed single or double bonds (π-bond orders 0 and 1) help open the band gap in that direction but are detrimental to their stability. Higher thermodynamic stability requires aggregating sp^2 regions together as it enhances delocalization. However, doing so with epoxides requires careful distribution so that the destabilizing steric repulsion from oxygen lone pairs is averted. The systematic inquiry into the isomeric C_4O nanosheets modeled here can be generalized to comprehensively understand the nature of π-delocalization and other electronic effects on the stabilities and band gaps of partially oxidized graphene, irrespective of the degree of saturation. The chemical insights drawn here for the assessment of thermodynamic stability and band gap engineering will help select a synthetic target that is appropriate for the particular requirement either through top-down[50] or bottom-up approaches[51] of atomistic controlled oxidation of graphene. It also provides a comprehensive understanding of the 2D π-delocalization in polycyclic benzenoid systems in terms of observable quantities instead of abstract resonance energy estimates.

■ ASSOCIATED CONTENT

Supporting Information

The Supporting Information is available free of charge at https://pubs.acs.org/doi/10.1021/acsomega.2c08169.

https://doi.org/10.1021/acsomega.2c08169
ACS Omega 2023, 8, 5124−5135

Optimized geometry of molecules along with interaction diagram, MOs and optimized geometry of C_4O nanosheets, phonon spectra, band structures, and DOS (PDF)

AUTHOR INFORMATION

Corresponding Author

Musiri M. Balakrishnarajan − *Chemical Information Sciences Lab, Department of Chemistry, Pondicherry University, Pondicherry 605014, India;* orcid.org/0000-0001-6863-346X; Email: mmbkr.che@pondiuni.edu.in

Authors

Gaurav Jhaa − *Chemical Information Sciences Lab, Department of Chemistry, Pondicherry University, Pondicherry 605014, India;* orcid.org/0000-0002-9600-6890

Pattath D. Pancharatna − *Chemical Information Sciences Lab, Department of Chemistry, Pondicherry University, Pondicherry 605014, India*

Complete contact information is available at: https://pubs.acs.org/10.1021/acsomega.2c08169

Notes

The authors declare no competing financial interest.

ACKNOWLEDGMENTS

P.D.P. acknowledges the funding by DST (grant no. CS-130/2016) by means of the Women Scientist Scheme (WOS-A) and G.J. acknowledges the Pondicherry University for the Institute Fellowship.

REFERENCES

(1) Rocke, A. J. Hypothesis and experiment in the early development of Kekulé's Benzene theory. *Ann. Sci.* **1985**, *42*, 355−381.

(2) Schleyer, P. v. R. Introduction: DelocalizationPi and Sigma. *Chem. Rev.* **2005**, *105*, 3433−3435.

(3) Kermack, W. O.; Robinson, R. LI.-An explanation of the property of induced polarity of atoms and an interpretation of the theory of partial valencies on an electronic basis. *J. Chem. Soc. Trans.* **1922**, *121*, 427−440.

(4) Pauling, L. The nature of the chemical bond. Application of results obtained from the quantum mechanics and from a theory of paramagnetic susceptibility to the structure of molecules. *J. Am. Chem. Soc.* **1931**, *53*, 1367−1400.

(5) Longuet-Higgins, H. C. Some Studies in Molecular Orbital Theory I. Resonance Structures and Molecular Orbitals in Unsaturated Hydrocarbons. *J. Chem. Phys.* **1950**, *18*, 265−274.

(6) Pancharatna, P. D.; Dar, S. H.; Chowdhury, U. D.; Balakrishnarajan, M. M. Anatomy of Classical Boron-Boron Bonding: Overlap and sp Dissonance. *J. Phys. Chem. A* **2022**, *126*, 3219−3228.

(7) White, M. A.; Kahwaji, S.; Freitas, V. L. S.; Siewert, R.; Weatherby, J. A.; Ribeiro da Silva, M. D. M. C.; Verevkin, S. P.; Johnson, E. R.; Zwanziger, J. W. The Relative Thermodynamic Stability of Diamond and Graphite. *Angew. Chem., Int. Ed. Engl.* **2021**, *60*, 1546−1549.

(8) Jarowski, P. D.; Wodrich, M. D.; Wannere, C. S.; Schleyer, P. v. R.; Houk, K. N. How Large Is the Conjugative Stabilization of Diynes? *J. Am. Chem. Soc.* **2004**, *126*, 15036−15037.

(9) Clar, E. The Aromatic Sextet. *Mobile Source Emissions Including Policyclic Organic Species*; Springer, 1983.

(10) Weiss, N. O.; Zhou, H.; Liao, L.; Liu, Y.; Jiang, S.; Huang, Y.; Duan, X. Graphene: An Emerging Electronic Material. *Adv. Mater.* **2012**, *24*, 5782−5825.

(11) Chaves, A.; Azadani, J. G.; Alsalman, H.; da Costa, D. R.; Frisenda, R.; Chaves, A. J.; Song, S. H.; Kim, Y. D.; He, D.; Zhou, J.; Castellanos-Gomez, A.; Peeters, F. M.; Liu, Z.; Hinkle, C. L.; Oh, S.-H.; Ye, P. D.; Koester, S. J.; Lee, Y. H.; Avouris, P.; Wang, X.; Low, T. Bandgap engineering of two-dimensional semiconductor materials. *npj 2D Mater. Appl.* **2020**, *4*, 29.

(12) Valli, A.; Amaricci, A.; Brosco, V.; Capone, M. Quantum Interference Assisted Spin Filtering in Graphene Nanoflakes. *Nano Lett.* **2018**, *18*, 2158−2164.

(13) Luo, H.; Yu, G. Preparation, Bandgap Engineering, and Performance Control of Graphene Nanoribbons. *Chem. Mater.* **2022**, *34*, 3588−3615.

(14) Gu, S.-Y.; Hsieh, C.-T.; Lin, T.-W.; Chang, J.-K.; Li, J.; Gandomi, Y. A. Tuning oxidation level, electrical conductance and band gap structure on graphene sheets by a cyclic atomic layer reduction technique. *Carbon* **2018**, *137*, 234−241.

(15) Mallick, B. C.; Hsieh, C.-T.; Yin, K.-M.; Li, J.; Ashraf Gandomi, Y. Linear control of the oxidation level on graphene oxide sheets using the cyclic atomic layer reduction technique. *Nanoscale* **2019**, *11*, 7833−7838.

(16) Ito, J.; Nakamura, J.; Natori, A. Semiconducting nature of the oxygen-adsorbed graphene sheet. *J. Appl. Phys.* **2008**, *103*, 113712.

(17) Nourbakhsh, A.; Cantoro, M.; Vosch, T.; Pourtois, G.; Clemente, F.; van der Veen, M. H.; Hofkens, J.; Heyns, M. M.; De Gendt, S.; Sels, B. F. Bandgap opening in oxygen plasma-treated graphene. *Nanotechnology* **2010**, *21*, 435203.

(18) Hossain, M. Z.; Johns, J. E.; Bevan, K. H.; Karmel, H. J.; Liang, Y. T.; Yoshimoto, S.; Mukai, K.; Koitaya, T.; Yoshinobu, J.; Kawai, M.; Lear, A. M.; Kesmodel, L. L.; Tait, S. L.; Hersam, M. C. Chemically homogeneous and thermally reversible oxidation of epitaxial graphene. *Nat. Chem.* **2012**, *4*, 305−309.

(19) Huang, H.; Li, Z.; She, J.; Wang, W. Oxygen density dependent band gap of reduced graphene oxide. *J. Appl. Phys.* **2012**, *111*, 054317.

(20) Pancharatna, P. D.; Jhaa, G.; Balakrishnarajan, M. M. Nature of Interactions between Epoxides in Graphene Oxide. *J. Phys. Chem. C* **2020**, *124*, 1695−1703.

(21) Porro, S.; Accornero, E.; Pirri, C. F.; Ricciardi, C. Memristive devices based on graphene oxide. *Carbon* **2015**, *85*, 383−396.

(22) Porro, S.; Ricciardi, C. Memristive behaviour in inkjet printed graphene oxide thin layers. *RSC Adv.* **2015**, *5*, 68565−68570.

(23) Yan, X.; Zhang, L.; Chen, H.; Li, X.; Wang, J.; Liu, Q.; Lu, C.; Chen, J.; Wu, H.; Zhou, P. Graphene Oxide Quantum Dots Based Memristors with Progressive Conduction Tuning for Artificial Synaptic Learning. *Adv. Funct. Mater.* **2018**, *28*, 1803728.

(24) Romero, F. J.; Toral-Lopez, A.; Ohata, A.; Morales, D. P.; Ruiz, F. G.; Godoy, A.; Rodriguez, N. Laser-Fabricated Reduced Graphene Oxide Memristors. *Nanomaterials* **2019**, *9*, 897.

(25) Frisch, M. J.; Trucks, G. W.; Schlegel, H. B.; Scuseria, G. E.; Robb, M. A.; Cheeseman, J. R.; Scalmani, G.; Barone, V.; Mennucci, B.; Petersson, G. A.; Nakatsuji, H.; Caricato, M.; Li, X.; Hratchian, H. P.; Izmaylov, A. F.; Bloino, J.; Zheng, G.; Sonnenberg, J. L.; Hada, M.; Ehara, M.; Toyota, K.; Fukuda, R.; Hasegawa, J.; Ishida, M.; Nakajima, T.; Honda, Y.; Kitao, O.; Nakai, H.; Vreven, T.; Montgomery, J. A., Jr; Peralta, J. E.; Ogliaro, F.; Bearpark, M.; Heyd, J. J.; Brothers, E.; Kudin, K. N.; Staroverov, V. N.; Kobayashi, R.; Normand, J.; Raghavachari, K.; Rendell, A.; Burant, J. C.; Iyengar, S. S.; Tomasi, J.; Cossi, M.; Rega, N.; Millam, J. M.; Klene, M.; Knox, J. E.; Cross, J. B.; Bakken, V.; Adamo, C.; Jaramillo, J.; Gomperts, R.; Stratmann, R. E.; Yazyev, O.; Austin, A. J.; Cammi, R.; Pomelli, C.; Ochterski, J. W.; Martin, R. L.; Morokuma, K.; Zakrzewski, V. G.; Voth, G. A.; Salvador, P.; Dannenberg, J. J.; Dapprich, S.; Daniels, A. D.; Farkas, Ö.; Foresman, J. B.; Ortiz, J. V.; Cioslowski, J.; Fox, D. J. *Gaussian 09* Rev. A.02; Gaussian, Inc.: Wallingford, CT, 2009.

(26) Clark, S. J.; Segall, M. D.; Pickard, C. J.; Hasnip, P. J.; Probert, M. I. J.; Refson, K.; Payne, M. C. First principles methods using CASTEP. *Z. Kristallogr. - Cryst. Mater.* **2005**, *220*, 567−570.

(27) Perdew, J. P.; Burke, K.; Ernzerhof, M. Generalized Gradient Approximation Made Simple. *Phys. Rev. Lett.* **1996**, *77*, 3865−3868.

(28) Perdew, J. P.; Wang, Y. Accurate and simple analytic representation of the electron-gas correlation energy. *Phys. Rev. B: Condens. Matter Mater. Phys.* **1992**, *45*, 13244−13249.
(29) Kohn, W.; Sham, L. J. Self-Consistent Equations Including Exchange and Correlation Effects. *Phys. Rev.* **1965**, *140*, A1133−A1138.
(30) Ceperley, D. M.; Alder, B. J. Ground State of the Electron Gas by a Stochastic Method. *Phys. Rev. Lett.* **1980**, *45*, 566−569.
(31) Monkhorst, H. J.; Pack, J. D. Special points for Brillouin-zone integrations. *Phys. Rev. B: Solid State* **1976**, *13*, 5188−5192.
(32) Hoffmann, R. An Extended Hückel Theory. I. Hydrocarbons. *J. Chem. Phys.* **1963**, *39*, 1397−1412.
(33) Mealli, C.; Proserpio, D. M. MO theory made visible. *J. Chem. Educ.* **1990**, *67*, 399.
(34) Marutheeswaran, S.; Pancharatna, P. D.; Balakrishnarajan, M. M. Preference for a propellane motif in pure silicon nanosheets. *Phys. Chem. Chem. Phys.* **2014**, *16*, 11186−11190.
(35) Marutheeswaran, S.; Pancharatna, P. D.; Balakrishnarajan, M. M. Density functional studies on (NCH)n azagraphane: activated surface for organocatalysis. *Phys. Chem. Chem. Phys.* **2014**, *16*, 19861−19865.
(36) Cyvin, S. J.; Gutman, I. *Kekulé Structures in Benzenoid Hydrocarbons*; Springer Berlin Heidelberg, 2013.
(37) Gutzler, R.; Perepichka, D. F. π-Electron Conjugation in Two Dimensions. *J. Am. Chem. Soc.* **2013**, *135*, 16585−16594.
(38) Hoffmann, R.; Heilbronner, E.; Gleiter, R. Interaction of nonconjugated double bonds. *J. Am. Chem. Soc.* **1970**, *92*, 706−707.
(39) Merchán, M.; Serrano-Andrés, L.; Slater, L. S.; Roos, B. O.; McDiarmid, R.; Xing. Electronic Spectra of 1,4-Cyclohexadiene and 1,3-Cyclohexadiene: A Combined Experimental and Theoretical Investigation. *J. Phys. Chem. A* **1999**, *103*, 5468−5476.
(40) Chang, Z.; Yan, W.; Shang, J.; Liu, J. Z. Piezoelectric properties of graphene oxide: A first-principles computational study. *Appl. Phys. Lett.* **2014**, *105*, 023103.
(41) Peierls, R. Zur Theorie der elektrischen und thermischen Leitfähigkeit von Metallen. *Ann. Phys.* **1930**, *396*, 121−148.
(42) Longuet-Higgins, H. C.; Salem, L. The alternation of bond lengths in long conjugated chain molecules. *Proc. R. Soc. London, Ser. A* **1959**, *251*, 172−185.
(43) Novak, I. Quantification of cross-conjugation. *Mol. Phys.* **2017**, *115*, 925−930.
(44) Solomon, G. C. Cross-Conjugation and Quantum Interference. *Cross Conjugation*; John Wiley & Sons, 2016; pp 397−412.
(45) Nozaki, D.; Toher, C. Is the Antiresonance in Meta-Contacted Benzene Due to the Destructive Superposition of Waves Traveling Two Different Routes around the Benzene Ring? *J. Phys. Chem. C* **2017**, *121*, 11739−11746.
(46) Kivelson, S.; Chapman, O. L. Polyacene and a new class of quasi-one-dimensional conductors. *Phys. Rev. B: Condens. Matter Mater. Phys.* **1983**, *28*, 7236−7243.
(47) Jiang, D.-e.; Dai, S. Electronic Ground State of Higher Acenes. *J. Phys. Chem. A* **2008**, *112*, 332−335.
(48) Yang, Y.; Davidson, E. R.; Yang, W. Nature of ground and electronic excited states of higher acenes. *Proc. Natl. Acad. Sci.* **2016**, *113*, E5098−E5107.
(49) Mallory, F. B.; Butler, K. E.; Evans, A. C.; Brondyke, E. J.; Mallory, C. W.; Yang, C.; Ellenstein, A. Phenacenes: A Family of Graphite Ribbons. 2. Syntheses of Some [7]Phenacenes and an [11]Phenacene by Stilbene-like Photocyclizations. *J. Am. Chem. Soc.* **1997**, *119*, 2119−2124.
(50) Rho, Y.; Grigoropoulos, C. P. A laser-based chemical process enables reversible doping of graphene. *Nat. Electron.* **2022**, *5*, 485−486.
(51) Poniatowska, A.; Trzaskowski, M.; Ciach, T. Production and properties of top-down and bottom-up graphene oxide. *Colloids Surf., A* **2019**, *561*, 315−324.

https://doi.org/10.1021/acsomega.2c08169
ACS Omega 2023, 8, 5124−5135